Available online at www.sciencedirect.com
ScienceDirect
Trans. Nonferrous Met. Soc. China 25(2015) 2556−2563
Transactions of Nonferrous Metals Society of China
www.tnmsc.cn

Corrosion behavior of Ti−Nb−Ta−Zr−Fe alloy for biomedical applications in Ringer's solution

Yan-fei XU[1], Yi-feng XIAO[1], Dan-qing YI[2], Hui-qun LIU[2], Liang WU[1], Jing WEN[1]

1. School of Mechanical Engineering, Xiangtan University, Xiangtan 411105, China;
2. School of Materials Science and Engineering, Central South University, Changsha 410083, China

Received 27 October 2014; accepted 20 March 2015

Abstract: The corrosion resistance of Ti−25Nb−10Ta−1Zr−0.2Fe (mass fraction, %) (TNTZF) alloy in Ringer's solution at 37 °C was investigated by potentiodynamic polarization measurement. Ti−6Al−4V ELI (Extra low interstitial) alloy was also investigated to make a comparison. The results show that TNTZF alloy has higher corrosion potential, lower corrosion current density, more stable passive current density and wider passive region compared with Ti–6Al–4V ELI alloy, which indicates that TNTZF alloy has better corrosion resistance. In addition, pitting corrosion is observed on the surface passive film of Ti–6Al–4V ELI alloy but is not found on that of TNTZF alloy. The XPS analysis results reveal that the passive film formed on TNTZF alloy is composed of Nb_2O_5, NbO_2, Ta_2O_5, ZrO_2, TiO and Ti_2O_3 oxides in the matrix of TiO_2, which makes the passive film more stable and protective than that formed on Ti−6Al−4V ELI alloy and contributes much to its superior corrosion resistance.
Key words: Ti alloy; biomaterials; corrosion behavior; passive film

1 Introduction

In comparison with the conventional stainless steels and Co-based alloys, Ti and its alloys exhibit more suitable characteristics for biomedical applications due to their low modulus and specific strength, superior biocompatibility and excellent corrosion resistance [1,2]. They are currently used as replacement materials for hard tissues such as artificial hip joints and dental implants. Pure Ti, Ti−6Al−4V ELI (Extra low interstitial) and Ti−6Al−7Nb alloys are most common α and $\alpha+\beta$ Ti materials used for medical applications up to date. But they are now found to be unsuitable for biomedical applications because of the toxic effect of both V and Al, and a relatively high elastic modulus (~120 GPa) when compared with that of human bone (10−30 GPa) [2,3]. β and metastable β types Ti alloys composed of nontoxic alloying elements, such as Nb, Ta, Mo, Zr, Sn and Fe, generally can be processed to higher strength level exhibiting lower elastic modulus and superior biocompatibility as compared with α and $\alpha+\beta$ types Ti alloys [4,5]. Metastable β alloys recently developed include Ti−12Mo−6Zr−2Fe [6], Ti−15Mo−3Nb−3O TTIMETAL 21SRx [7] and Ti−13Nb−13Zr [8], etc. More recently, Ti−29Nb−13Ta−4.6Zr, Ti−35Nb−5Ta−7Zr, Ti−24Nb−4Zr−7.9Sn and several other compositions have been received considerable attention and investigated extensively [9−11].

To determine the suitability of a material for body implant applications, several properties must be evaluated, such as mechanical, wear, fatigue and corrosion properties. Among these properties, the corrosion behavior is of crucial importance for the longevity of the material in the human system. Since the environment of human body is extremely complicated electrolyte containing many erosive species. The low corrosion resistance of the implants in the body fluid results in the release of noncompatible metal ions from the implants into the surrounding tissues, which may cause allergic and toxic reactions and finally lead to mechanical failure of the implants [12]. Alloying of certain elements along with Ti is found to offer a better corrosion resistance in acidic solution [13−16]. Ti with the addition of Pd offers better corrosion resistance than pure Ti in the phosphate buffered saline solutions

Foundation item: Project (51401175) supported by the National Natural Science Foundation of China; Project (13C902) supported by the Scientific Research Fund of Education Department of Hunan Province, China; Project (2015JJ3123) supported by the Natural Science Foundation of Hunan Province, China
Corresponding author: Yi-feng XIAO; Tel: +86-731-58292064; E-mail: xiaoyifeng@xtu.edu.cn
DOI: 10.1016/S1003-6326(15)63875-4

containing H_2O_2 [13]. Ti−12Mo−5Zr alloy also has better corrosion properties than Ti−6Al−4V and is comparable to the pure Ti in Hank's solution [14]. YU et al [15] reported that the additions of Nb and Zr can increase the thermodynamic or kinetic stability of Ti, and thus reduce the active anodic dissolution rates in HCl solutions and enhance the passivation in comparison with pure Ti.

A new metastable β type Ti alloy Ti−25Nb−10Ta−1Zr−0.2Fe (mass fraction, %) (TNTZF) has been developed for potential implant material recently. Compared with the most currently used Ti-based biomaterial Ti−6Al−4V ELI, TNTZF alloy has advantages of ultra-low elastic modulus, high strength and composition of nontoxic alloying elements [17,18]. Therefore, this study focuses on the corrosion behavior of TNTZF alloy in Ringer's solution using electrochemical measurement and XPS analysis. For comparison, the same measurements are also performed on Ti−6Al−4V ELI alloy used as standard biomaterials.

2 Experimental

2.1 Material preparation

A Ti alloy with a nominal composition of Ti−25Nb−10Ta−1Zr−0.2Fe (mass fraction, %) (TNTZF) was designed for potential implant material according to the principle of nontoxic and low elastic modulus [17,18]. The TNTZF ingot was fabricated using high purity sponge Ti and Zr, Ti−21Ta interalloy and high purity Nb and Fe as raw materials. Owing to the big difference in melting points and densities among these raw materials, the ingot was first made by electron beam furnace, followed by vacuum consumable arc melting. The obtained ingot was mechanically cleaned in order to remove the oxide layer and homogenized at 1200 °C for 12 h under vacuum condition, and then freely forged into a quadrate slab (250 mm × 155 mm × 35 mm). After annealing at 850 °C for 40 min, the alloy was hot rolled from 35 mm to 10 mm in thickness by six passes without reheating. The hot rolled plate was solution treated at 900 °C for 1 h in argon followed by water quenching and then cut into several plates for electrochemical test.

The specimens of TNTZF and as-received Ti−6Al−4V ELI alloys with dimensions of 10 mm × 10 mm × 3 mm were connected to a Cu wire and embedded in an epoxy cold resin mounting with surface area of 1 cm^2 exposed to the Ringer's solution. The exposed surface of specimen was mechanically ground with silicon carbide paper until 1400 grit, and then ultrasonically degreased in acetone, cleaned in distilled water and finally dried in air.

2.2 Electrochemical tests

The electrochemical measurements were carried out on a ZAHNER IM6eX electrochemical workstation. The specimen, a Pt plate and a saturated calomel electrode (SCE) were used as the working electrode, counter electrode and reference electrode, respectively. Ringer's solution with chemical compositions of 9 g/L NaCl, 0.42 g/L KCl, 0.2 g/L $NaHCO_3$ and 0.25 g/L $CaCl_2$ was used as the electrolyte solution. The Ringer's solution was commonly used to simulate human body fluid condition for evaluating the corrosion characteristics of implant materials [19]. The pH value of the solution was maintained at 7.2 by adding HCl or NaOH. The potentiodynamic polarization of the specimen was recorded in a scan range of −500 to +2500 mV (vs SCE) at a scan rate of 2 mV/s after 1 h immersion in the electrolyte. In every test, the medium was maintained at 37 °C. Three specimens were tested for each condition.

2.3 Material characterization

The microstructures of as-received Ti−6Al−4V ELI and solution treated TNTZF alloys were observed by optical microscopy (OM). The phase constitution was analyzed by X-ray diffraction (XRD) using a Rigaku D/Max 2500 diffractometer with Cu K_α radiation and graphite monochromator operated at 40 kV and 250 mA.

After corrosion tests, the surface morphologies of the alloys were observed on an FEI Sirion 200 scanning electron microscope (SEM) operated at 20 kV. The chemical compositions of the passive films were characterized by a Thermo Fisher Scientific K_α 1063 photoelectron spectroscope (XPS) coupled with a monochromatic Al K_α X-ray source under vacuum pressure of ~10^{-7} Pa. The X-ray voltage and power were 12 kV and 72 W, respectively. The binding energy was calibrated using C 1s hydrocarbon peak at 284.8 eV. The surface of specimen was sputtered by an Ar^+ ion beam for 1 min prior to the XPS analysis to remove the surface contamination.

3 Results and discussion

Figure 1 shows the optical microstructures of as-received Ti−6Al−4V ELI and solution treated TNTZF alloys. It is clear that Ti−6Al−4V ELI alloy exhibits a typical 'basket-weave' morphology consisting of lamellar α colonies in prior β grains, as shown in Fig. 1(a). TNTZF alloy has equiaxed grains with the size in the range of 50−150 μm (Fig. 1(b)). The XRD patterns also confirm that Ti−6Al−4V ELI alloy is composed of α and β phases and the solution treated TNTZF alloy consists of only single β phase, as shown in Fig. 2.

Figure 3 shows the potentiodynamic polarization curves of TNTZF and Ti−6Al−4V ELI alloys in Ringer's solution at 37 °C. Both the polarization curves show a

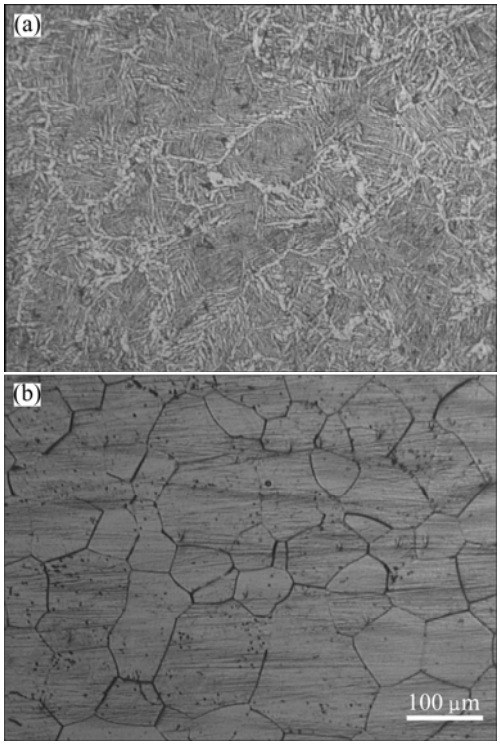

Fig. 1 Optical micrographs of Ti−6Al−4V ELI (a) and TNTZF (b) alloys

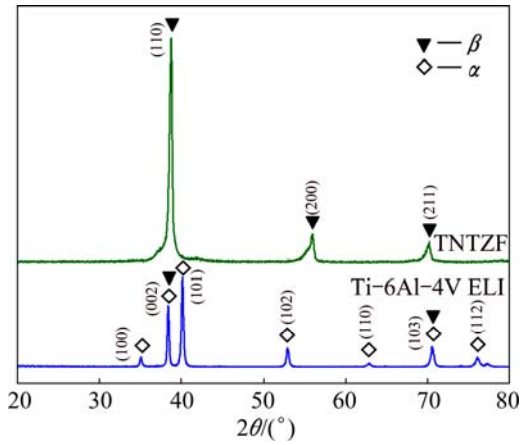

Fig. 2 XRD patterns of Ti−6Al−4V ELI and TNTZF alloys

similar variation trend and can be divided into four regions. In the first region (Region *a*), the current density increases with increasing the potential. Both alloys exhibit a typical activation polarization and show a well defined linear relationship between the potential and the current density in the Tafel regions. The corrosion potentials (φ_{corr}) and corrosion current densities (J_{corr}) are obtained by Tafel extrapolation analysis using both anodic and cathodic branches of the curves [20]. The results show that the values of φ_{corr} for Ti−6Al−4V ELI and TNTZF alloys are about −125.5 and −71.7 mV (vs SCE), respectively. The J_{corr} value of TNTZF alloy is ~0.22 μA/cm^2, which is lower than that of Ti−6Al−4V ELI of ~0.31 μA/cm^2. Afterwards, the electrodes transfer from the active-passive state to the passive state in the region *b*. In this region, the current densities of TNTZF alloy remain very stable in a wide passive region of 470 to 1680 mV (vs SCE), which indicates that a stable passive film is steadily formed. In contrast, the relatively stable current density of Ti−6Al−4V ELI is achieved in the early stage of this region suggesting the formation of a passive film, and then continuous oscillations of current density occur in the range of 970−1620 mV (vs SCE). The oscillations of current density could be related to the nucleation and repassivation of metastable pits in the passive film [21]. The passive current density (J_p) of TNTZF alloy is ~8.46 μA/cm^2, which is lower than that of Ti−6Al−4V ELI of ~12.35 μA/cm^2. After that, a slow increase of current density with increasing the potential can be observed for both alloys in the region *c*, which should be attributed to the breakdown of passive films by chlorine ions from the solution. With further increasing the potential, the current densities stabilize again in the region *d*, which means passive films change into the re-passive state. It is clear that the restoration time for the passive film of TNTZF alloy is shorter than that of Ti−6Al−4V ELI alloy, which suggests that the passive film formed on the surface of TNTZF alloy is more stable and protective than that of Ti−6Al−4V ELI alloy. The above electrochemical parameters are listed in Table 1.

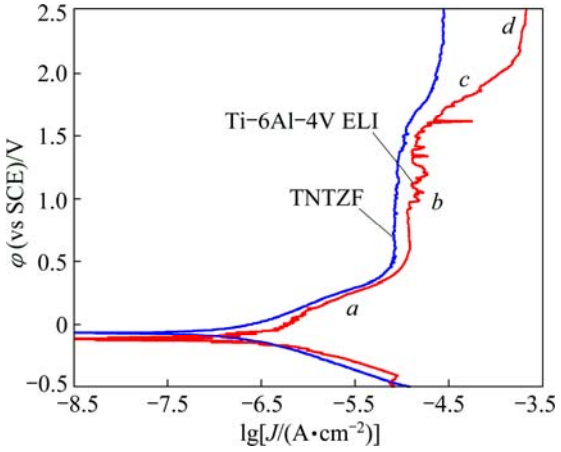

Fig. 3 Potentiodynamic polarization curves of Ti−6Al−4V ELI and TNTZF alloys in Ringer's solution at 37 °C

Table 1 Corrosion parameters of Ti−6Al−4V ELI and TNTZF alloys in Ringer's solution at 37 °C

Alloy	φ_{corr}/ mV	J_{corr}/ (μA·cm^{-2})	J_p/ (μA·cm^{-2})
Ti−6Al−4V ELI	−125.5	0.31	12.35
TNTZF	−71.7	0.22	8.46

From the polarization curves and the corrosion parameters listed in Table 1, it can be judged that in comparison with Ti−6Al−4V ELI alloy, TNTZF has

higher corrosion potential, lower corrosion current density, lower and more stable passive current densities and wider passive region, indicating that TNTZF alloy possesses better corrosion resistance in Ringer's solution.

The surface morphologies of Ti−6Al−4V ELI and TNTZF alloys after polarization test in Ringer's solution are shown in Fig. 4. There is obvious difference on the surface morphologies between Ti−6Al−4V ELI and TNTZF alloys. A lot of small pits over the surface are observed for Ti−6Al−4V ELI alloy, as indicated by arrows in Fig. 4(a), but few pits can be found on the surface of TNTZF alloy (Fig. 4(b)). This confirms that TNTZF alloy has better corrosion resistance than Ti−6Al−4V ELI alloy, which is in good agreement with the polarization results shown in Fig. 3. Pitting corrosion was often observed on the surfaces of pure Ti and its alloys after anodic tests in chloride solutions [22]. Pitting is a localized attack that results in rapid electrolyte penetration and removal of film and substrate at small areas. In the presence of chloride, Cl^- can migrate in parallel across the passivating oxide. Thus, if Cl^- reaches the metal/film interface, it would accelerate the anodic dissolution of TiO_2/Ti and form the metal chloride (or perhaps in the case of titanium, metal oxychloride). The accumulation of metal chloride at the metal/film interface may cause oxide film rupture, resulting in the nucleation of pits [22].

Figure 5 shows the XPS spectra for the passive film formed on the surface of Ti−6Al−4V ELI alloy after polarization in Ringer's solution. The wide scanning spectrum of the passive film is shown in Fig. 5(a), which confirms the presence of Ti, O, Al, V, C and Ar. The peaks of C 1s and Ar 2p observed in the spectrum can be attributed to the surface contamination of specimen during experiments. Quantitative analysis of XPS reveals that the chemical composition is 26.6% Ti, 5.9% Al, 0.8% V and 66.7% O (mole fraction). It suggests that the passive film consists predominantly of Ti oxides.

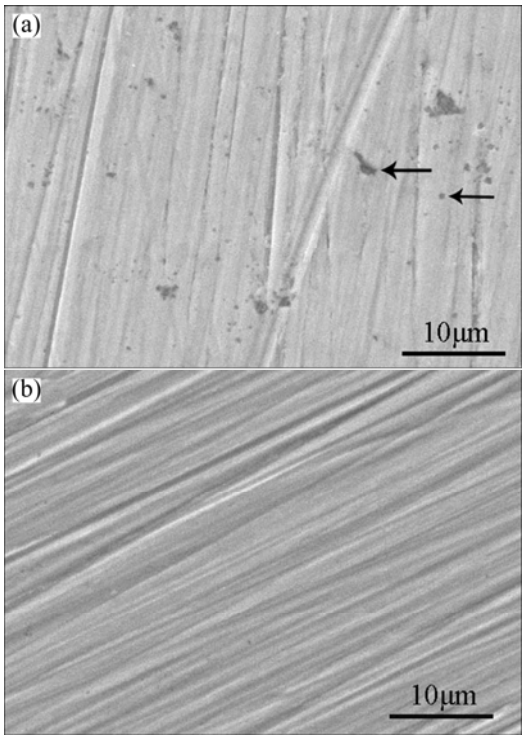

Fig. 4 Surface SEM morphologies of Ti−6Al−4V ELI (a) and TNTZF (b) alloys after polarization test

The narrow scanning spectrum of Ti 2p (Fig. 5(b)) can be decomposed into three doublet peaks which are assigned to oxidation states Ti^{4+}, Ti^{3+} and Ti^{2+}, corresponding to TiO_2, Ti_2O_3 and TiO, respectively. Quantitative analysis of XPS indicates that the majority of titanium (78%) is in the form of TiO_2 (Ti^{4+}), 15% as Ti_2O_3 (Ti^{3+}) and the rest (7%) is in TiO (Ti^{2+}) state. This result is consistent with the previous report [16] that TiO_2 was predominant in the passive oxide layers on Ti alloy and a small amount of sub-oxides TiO and Ti_2O_3 were also observed at the inner metal/oxide interface. In the case of Al 2p (Fig. 5(c)), the centre of the peak is located at 74.2 eV, thus denoting the formation of Al_2O_3 [16]. Figure 5(d) shows the narrow scanning spectrum of V 2p spectrum which can be fitted to a doublet peak with a single peak. The doublet peak located at 512.5 and 520.4 eV are in association with the $2p_{3/2}$ and $2p_{1/2}$ of metallic vanadium (V^0), respectively, while the single peak at 515.0 eV corresponding to V^{3+}, as previously reported [23]. Thus, this result confirms the presence of V_2O_3 in the surface passive film. As shown in Fig. 5(e), the peak of the O 1s can be separated into mainly two peaks: the primary peak located at 530.5 eV originating from O^{2-} ions in oxide, and the minor peak at 531.8 eV corresponding to hydroxyl groups, OH^- [24]. Based on the results of XPS, the passive film formed on the surface of Ti−6Al−4V ELI alloy is predominately TiO_2 with a small amount of TiO, Ti_2O_3, Al_2O_3 and V_2O_3.

Figure 6 shows the XPS spectra for the passive film formed on the surface of TNTZF alloy after polarization in Ringer's solution. Apart from the peak of C, the peaks of Ti, Nb, Ta, Zr and O are observed in the wide scanning spectrum, as shown in Fig. 6(a). The peak of Fe can not be detected in the wide scanning spectrum due to the small amount of Fe in the alloy. The chemical composition is 23.6% Ti, 6.4% Nb, 0.8% Ta, 0.9% Zr and 68.3% O (mole fraction). It suggests that the passive film of TNTZF alloy is also predominantly composed of Ti oxides.

Figure 6(b) is the narrow scanning spectrum of Ti 2p of TNTZF alloy, which shows a similar shape to that of Ti−6Al−4V ELI alloy. This spectrum is also composed of three doublets corresponding to TiO_2, Ti_2O_3 and TiO. The relative contents of TiO_2 (Ti^{4+}), Ti_2O_3 (Ti^{3+}) and TiO (Ti^{2+}) are calculated to be 83%, 13% and 4%, respectively, according to quantitative analysis of XPS.

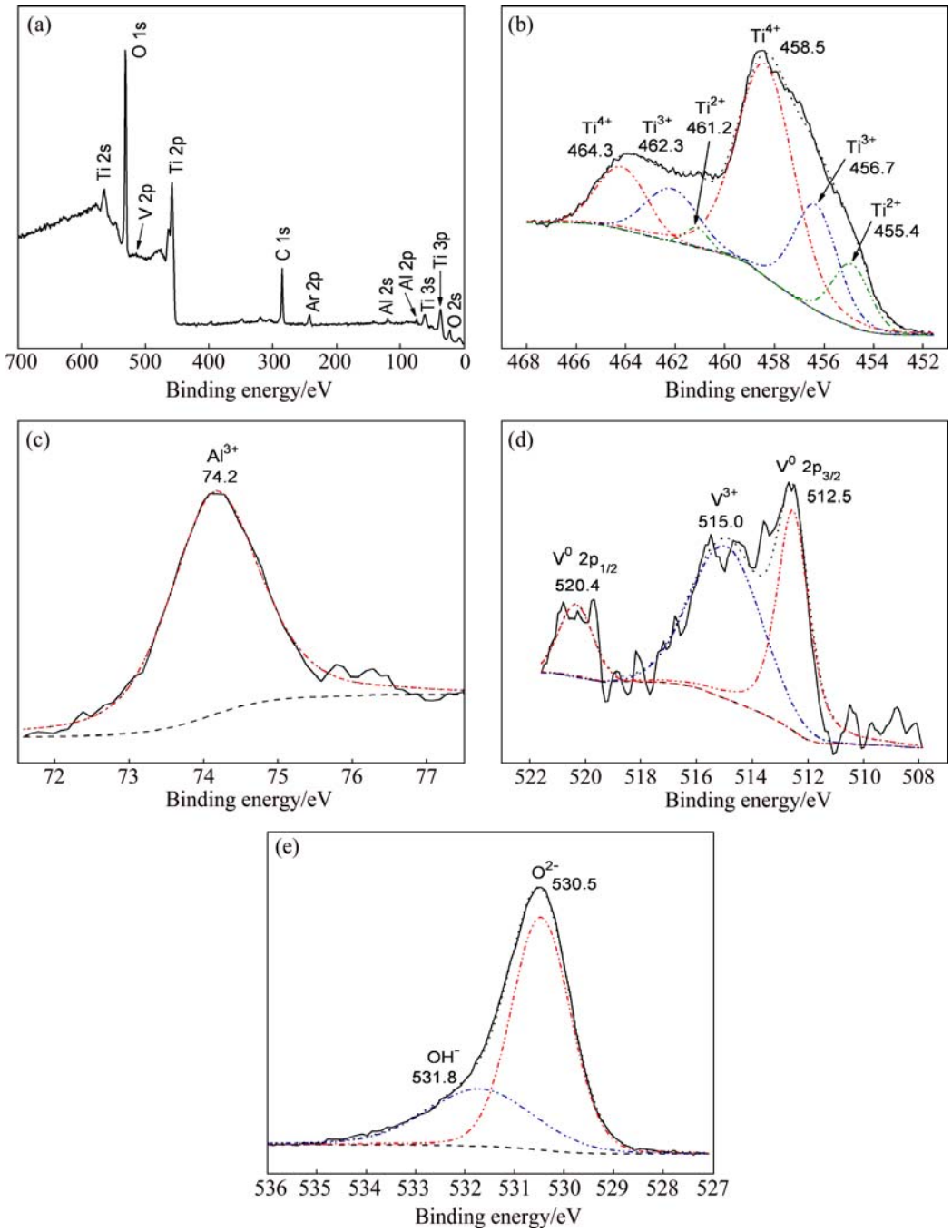

Fig. 5 XPS spectra of surface of Ti−6Al−4V ELI alloy after polarization test: (a) Wide scanning; (b) Ti 2p; (c) Al 2p; (d) V 2p; (e) O 1s spectra

This indicates that TiO_2 is also the predominant oxide of the passive film of TNTZF alloy. The narrow scanning spectrum of Nb 3d (Fig. 6(c)) can be separated into a singlet peak and a doublet peak, which are corresponding to Nb^{4+} and Nb^{5+} states, respectively. This suggests that the Nb oxides NbO_2 and Nb_2O_5 are formed in the passive film, the latter is predominant due to the fact that the relative content is $n(Nb^{5+})(Nb_2O_5):n(Nb^{4+})(NbO_2)$=75:25. The peaks of Ta 4f spectrum (Fig. 6(d)) are located at about 26.1 and 27.9 eV, which can be assigned to $4f_{7/2}$ and $4f_{5/2}$ core levels of Ta^{5+}, respectively [16]. This indicates that Ta exists in the oxide film as Ta_2O_5. The Zr 3d spectrum is composed of a doublet peak corresponding to $3d_{5/2}$ (182.4 eV) and $3d_{3/2}$ (184.9 eV) electrons of Zr^{4+}, as shown in Fig. 6(e). These binding energy values are in agreement with those reported in the literature for ZrO_2 [25]. Similarly to that of Ti−6Al−4V ELI alloy, the spectrum of O 1s of TNTZF alloy also consists of two peaks corresponding to O^{2-} and OH^- (Fig. 6(f)). Thus, the above XPS analyses confirm that,

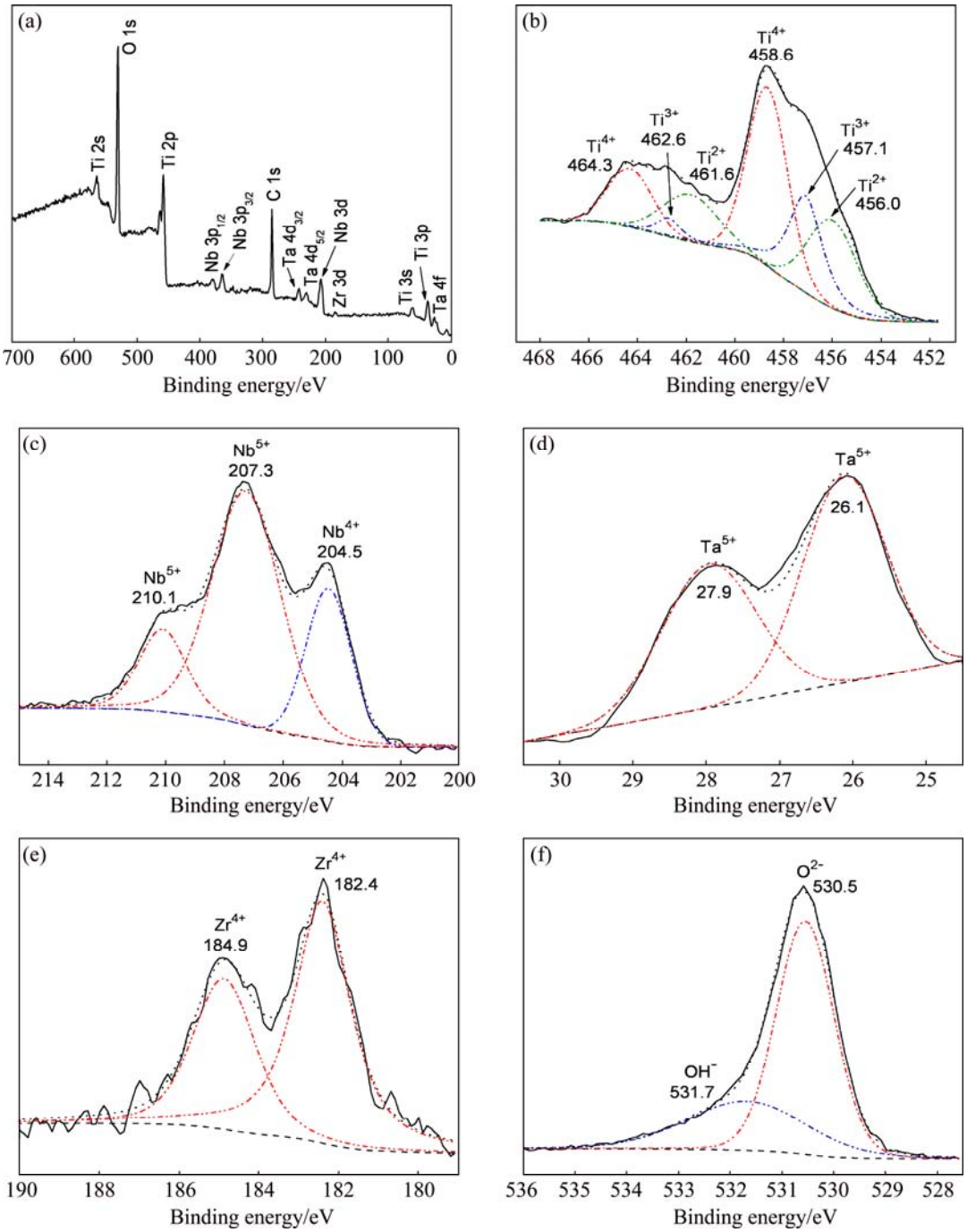

Fig. 6 XPS spectra of surface of TNTZF alloy after polarization test: (a) Wide scanning; (b) Ti 2p; (c) Nb 3d; (d) Ta 4f; (e) Zr 3d; (f) O 1s

in addition to TiO and Ti_2O_3, there are Nb_2O_5, NbO_2, Ta_2O_5 and ZrO_2 oxides in the TiO_2 matrix in the passive film formed on the surface of TNTZF alloy.

The corrosion resistance of metals and alloys depends on several factors, such as composition, environment and microstructure. In the present study, TNTZF alloy exhibits a better corrosion resistance than Ti−6Al−4V ELI, which can be mainly attributed to the additions of Nb, Ta and Zr elements in the alloy, resulting in the formation of a more stable and inert oxide film (mainly composed of TiO_2, Nb_2O_5, NbO_2, Ta_2O_5 and ZrO_2) on the surface of TNTZF alloy. According to YU et al [15], the additions of both Nb and Zr to Ti resulted in a ternary alloy with extremely high resistance to active and passive dissolution in oxidizing acids. They explained the beneficial effect of Nb or Zr alloying on the corrosion resistance through the formation of strong covalent bonds between near neighbors Ti, Nb and Zr by sharing the unpaired d-level electron [15]. The addition of Ta can improve the

resistance of Ti alloys in the chloride solutions because pure Ta is resistant to chlorine due to relatively stable Ta_2O_5 oxide film. Therefore, as observed in Fig. 4(b), TNTZF alloy exhibiting a superior resistance to pitting corrosion can be attributed to the presence of Nb_2O_5, NbO_2, Ta_2O_5 and ZrO_2 oxides in the passive TiO_2 layer, which can restrain Cl^- ingress into the oxide layer and improve the structural integrity of the oxide film, thereby reducing the initiation of pits. In contrast, the inferior pitting corrosion does occur for Ti−6Al−4V ELI alloy, as observed in Fig. 4(a). This is attributable to the additions of Al and V elements which can significantly diminish the pitting resistance of Ti alloys [26]. It was also reported that localized corrosion of Ti−6Al−4V ELI alloy was related to the dissolution of V oxide at the surface film/electrolyte interface in Cl^--containing solutions [27]. Moreover, Ta, Zr and Nb ions have lower solubility than Al and V ions in aqueous media [28], indicating that the passive film of TNTZF alloy is more stable and difficult to dissolve into the solution compared with that of Ti−6Al−4V ELI alloy.

On the other hand, the distribution of alloying elements in different phases also influences the corrosion resistance of these two alloys to some extent. Previous studies showed that the structural and chemical differences between α and β phases of Ti alloys caused galvanic interaction, which led to the formation of unstable passive layer and the acceleration of corrosion [29]. HE et al [30] reported that the large difference in composition between α and β phases caused the different rates of film formation on α and β phases, which resulted in film fracture at the α/β interfaces thereby initiating corrosion attack. Thus, the segregation of β-stabilizer V to β phase and α-stabilizer Al to α phase in Ti−6Al−4V ELI alloy probably causes the galvanic interaction between α and β phases and the preferential dissolution of α/β interfaces. This viewpoint can be approved by the previous reports that localized corrosion often initiated at the α/β interface in Ti−6Al−4V ELI alloy [31]. In contrast, pitting corrosion hardly occurs in TNTZF alloy with the microstructure of single β phase, in which alloying elements distribute more uniformly.

Therefore, the corrosion resistance of TNTZF alloy is much better than that of Ti–6Al–4V ELI alloy used as a standard biomaterial, suggesting promising potential of TNTZF alloy for biomedical applications from the viewpoint of excellent corrosion resistance.

4 Conclusions

1) TNTZF alloy has higher corrosion potential, lower and more stable passive current densities and wider passive region than Ti−6Al−4V ELI, indicating that TNTZF alloy possesses much better corrosion resistance.

2) A lot of small pits are observed on the surface of Ti−6Al−4V ELI alloy but almost no pits can be found on that of TNTZF alloy.

3) Based on the results of XPS, the passive film formed on the surface of TZNTF alloy is composed of Nb_2O_5, NbO_2, Ta_2O_5, ZrO_2, TiO and Ti_2O_3 oxides in the matrix of TiO_2, which makes the passive film more stable and protective than that formed on Ti−6Al−4V ELI alloy and contributes much to its superior corrosion resistance.

References

[1] NIINOMI M. Recent metallic materials for biomedical applications [J]. Metallurgical and Materials Transactions A, 2002, 33: 477−486.

[2] GEETHA M, SINGH A K, ASOKAMANI R, GOGIA A K. Ti based biomaterials, the ultimate choice for orthopaedic implants—A review [J]. Progress in Materials Science, 2009, 54: 397−425.

[3] NIINOMI M. Mechanical properties of biomedical titanium alloys [J]. Materials Science and Engineering A, 1998, 243: 231−236.

[4] ZHANG Y W, LI S J, OBBARD E G, WANG H, WANG S C, HAO Y L, YANG R. Elastic properties of Ti−24Nb−4Zr−8Sn single crystals with BCC crystal structure [J]. Acta Materialia, 2011, 59: 3081−3090.

[5] DAI Shi-juan, WANG Yu, CHEN Feng, YU Xin-quan, ZHANG You-fa. Influence of Zr content on microstructure and mechanical properties of implant Ti−35Nb−4Sn−6Mo−*x*Zr alloys [J]. Transactions of Nonferrous Metals Society of China, 2013, 23(5): 1299−1303.

[6] WANG K, GUSTAVSON L, DUMBLETON J. The characterization of Ti−12Mo−6Zr−2Fe: A new biocompatible titanium alloy developed for surgical implants [C]//Beta titanium in the 1990's. Warrendale: The Minerals, Metals & Materials Society, 1993: 49−60.

[7] FANNING J C. Properties and processing of a new metastable beta titanium alloy for surgical implant applications: TIMETAL™ 21SRx [C]//Titanium 95' Science and Technology. London: Institute of Materials, 1996: 1800−1807.

[8] MAJUMDAR P, SINGH S B, CHAKRABORTY M. The role of heat treatment on microstructure and mechanical properties of Ti–13Zr–13Nb alloy for biomedical load bearing applications [J]. Journal of the Mechanical Behavior of Biomedical Materials, 2011, 4: 1132−1144.

[9] YILMAZER H, NIINOMI M, NAKAI M, HIEDA J, TODAKA Y, AKAHORI T, MIYAZAKI T. Heterogeneous structure and mechanical hardness of biomedical β-type Ti–29Nb–13Ta–4.6Zr subjected to high-pressure torsion [J]. Journal of the Mechanical Behavior of Biomedical Materials, 2012, 10: 235−245.

[10] AFONSO C R M, FERRANDINI P L, ANTONIO A J, CARAM R. High resolution transmission electron microscopy study of the hardening mechanism through phase separation in a β-Ti–35Nb–7Zr–5Ta alloy for implant applications [J]. Acta Biomaterialia, 2010, 6: 1625−1629.

[11] BAI Y, LI S J, PRIMA F, HAO Y L, YANG R. Electrochemical corrosion behavior of Ti−24Nb−4Zr−8Sn alloy in a simulated physiological environment [J]. Applied Surface Science, 2012, 258: 4035−4040.

[12] HALLAB N J, ANDERSON S, STAFFORD T, GLANT T, JACOBS J J. Lymphocyte responses in patients with total hip arthroplasty [J]. Journal of Orthopaedic Research, 2005, 23(2): 384−391.

[13] HANDZLIK P, FITZNER K. Corrosion resistance of Ti and Ti−Pd

alloy in phosphate buffered saline solutions with and without H_2O_2 addition phosphate buffered saline (PBS) solutions [J]. Transactions of Nonferrous Metals Society of China, 2013, 23(3): 866−875.

[14] ZHAO C L, ZHANG X N, CAO P. Mechanical and electrochemical characterization of Ti−12Mo−5Zr alloy for biomedical application [J]. Journal of Alloys and Compounds, 2011, 509: 8235−8238.

[15] YU S Y, SCULLY J R, VITUS C M. Influence of niobium and zirconium alloying additions on the anodic dissolution behavior of activated titanium in HCl solutions [J]. Journal of the Electrochemical Society B, 2001, 148(2): 68−78.

[16] OKAZAKI Y, KYO K, ITO Y, TATEISHI T. Effects of Mo and Pd on corrosion resistance of V-free titanium alloys for medical implants [J]. Materials Transactions, 1997, 38: 344−352.

[17] XU Y F, YI D Q, LIU H Q, WANG B, YANG F L. Age-hardening behavior, microstructural evolution and grain growth kinetics of isothermal ω phase of Ti−Nb−Ta−Zr−Fe alloy for biomedical applications [J]. Materials Science and Engineering A, 2011, 529: 326−334.

[18] XU Y F, YI D Q, LIU H Q, WU X Y, WANG B, YANG F L. Effects of cold deformation on microstructure, texture evolution and mechanical properties of Ti−Nb−Ta−Zr−Fe alloy for biomedical applications [J]. Materials Science and Engineering A, 2012, 547: 64−71.

[19] CVIJOVIC-ALAGIC I, CVIJOVIC Z, MITROVIC S, PANIC V, RAKIN M. Wear and corrosion behaviour of Ti–13Nb–13Zr and Ti−6Al−4V alloys in simulated physiological solution [J]. Corrosion Science, 2011, 53: 796−808.

[20] McCAFFERTY E. Validation of corrosion rates measured by the Tafel extrapolation method [J]. Corrosion Science, 2005, 47: 3202−3215.

[21] PRIDE S T, SCULLY J R, HUDSON J L. Metastable pitting of aluminum and criteria for the transition to stable pit growth [J]. Journal of the Electrochemical Society, 1994, 141(11): 3028−3040.

[22] BURSTEIN G T, LIU C, SOUTO R M. The effect of temperature on the nucleation of corrosion pits on titanium in Ringer's physiological solution [J]. Biomaterials, 2005, 26: 245−256.

[23] RAO C N R, SARMA D D, VASUDEVAN S, HEGDE M S. Study of transition metal oxides by photoelectron spectroscopy [J]. Proceeding of Royal Society of London A, 1979, 367: 239−252.

[24] TANAKA Y, NAKAI M, AKAHORI T, NIINOMI M, TSUTSUMI Y, DOI H, HANAWA T. Characterization of air-formed surface oxide film on Ti−29Nb−13Ta−4.6Zr alloy surface using XPS and AES [J]. Corrosion Science, 2008, 50: 2111−2116.

[25] CABELLO G, LILLO L, BUONO-CORE G E. Zr(IV) and Hf(IV) β-diketonate complexes as precursors for the photochemical deposition of ZrO_2 and HfO_2 thin films [J]. Journal of Non-Crystalline Solids, 2008, 354: 982−988.

[26] KOLMAN D G, SCULLY J R. Electrochemistry and passivity of Ti−15V−3Cr−3Al−3Sn β-titanium alloy in ambient temperature aqueous chloride solution [J]. Journal of the Electrochemical Society, 1994, 142(10): 2633−2641.

[27] METIKOS-HUKOVIC M, KWOKAL A, PILJAC J. The influence of niobium and vanadium on passivity of titanium-based implants in physiological solution [J]. Biomaterials, 2003, 24: 3765−3775.

[28] ZHOU Y L, NIINOMI M, AKAHORI T, FUKUI H, TODA H. Corrosion resistance and biocompatibility of Ti–Ta alloys for biomedical applications [J]. Materials Science and Engineering A, 2005, 398: 28−36.

[29] LEVY M, SKLOVER G. Anodic polarization of titanium and titanium alloys in hydrochloric acid [J]. Journal of the Electrochemical Society, 1969, 116(1): 323−328.

[30] HE X, NOEL J J, SHOESMITH D W. Effects of iron content on microstructure and crevice corrosion of Grade-2 titanium [J]. Corrosion, 2004, 60: 378−385.

[31] CODARO E N, NAKAZATO R Z, HOROVISTIZ A L, RIBEIRO L M F, RIBEIRO R B, HEIN L R O. An image analysis study of pit formation on Ti−6Al−4V [J]. Materials Science and Engineering A, 2003, 341: 202−210.

生物医用 Ti−Nb−Ta-Zr-Fe 合金在林格溶液中的腐蚀行为

许艳飞[1]，肖逸锋[1]，易丹青[2]，刘会群[2]，吴 靓[1]，文 璟[1]

1. 湘潭大学 机械工程学院，湘潭 411105；
2. 中南大学 材料科学与工程学院，长沙 410083

摘 要：采用动电位极化方法研究 Ti−25Nb−10Ta−1Zr−0.2Fe (质量分数，%)(TNTZF) 合金 37 ℃ 下在林格溶液中的抗腐蚀性能，并在同样的条件下用 Ti−6Al−4V ELI(低间隙)合金做对比实验。结果表明：TNTZF 比 Ti−6Al−4V ELI 合金表现出更高的腐蚀电位，更低的腐蚀电流密度，更加稳定的钝化电流密度和更宽的钝化区间，因此具有更加优越的抗腐蚀性能。除此之外，在 Ti−6Al−4V ELI 合金的表面钝化膜上观察到了点蚀现象，但是在 TNTZF 合金表面没有发现点蚀现象。XPS 分析结果表明：TNTZF 合金表面钝化膜由 TiO_2 基体以及 Nb_2O_5、NbO_2、Ta_2O_5、ZrO_2、TiO 和 Ti_2O_3 等氧化物共同组成，从而使得钝化膜更加稳定且保护作用更强，因此 TNTZF 合金比 Ti−6Al−4V ELI 合金表现出更加优越的抗腐蚀性能。

关键词：钛合金；生物医用材料；腐蚀行为；钝化膜

(Edited by Mu-lan QIN)